OPEN ACCESS Freely available online

Journal of Aeronautics and Aerospace Engineering

Research Article

# Influence of Micro-Blowing Technique Hole Parameters on Drag Reduction of Civil Aircraft Engine Nacelle: A Computational Study

**Mushfiq Al Arafa*, Macdonald Mutekwa, Zhaolin Chen**
*Department of Science, Computational Engineering, University of Dhaka, Dhaka, Bangladesh*

## ABSTRACT

The numerical parametric analysis conducted to analyze the impact of Micro-Blowing Technique (MBT) whole-parameters is quite few at the present stage. The main aim of this research paper is to analyze the effect of micro blowing flow rate and its different hole-parameters on the skin friction drag reduction of an aircraft engine nacelle operating at cruise conditions. The primary tasks are focused to understand the behavior of the flow characteristics at the vicinity of the micro-porous holes by means of different types of MBT configurations. The interaction between main-stream flow and the micro-channel flow is numerically solved by using the Reynolds average Navier-Stokes equation and the k-omega SST is used to model the turbulent flow at the vicinity of the wall region. The hole-pattern is kept aligned in a single-row channel and the shape of the whole cross-section is kept straight to obtain an overall simplicity of the simulation model. The influences of the micro blowing technique are quite clearly seen from the simulation results, as there is a significant reduction in the velocity gradient between the solid engine nacelle surface and all the MBT configurations. The porous engine nacelle surface with zero blowing velocity is capable to reduce the skin friction drag by 7.045 % than of its solid surface, implying that the presence of the micro-porous holes possesses low effective surface roughness and it is an effective method to manipulate the turbulent boundary layer. The optimum skin friction drag reduction is observed when the geometrical characteristics of the holes possess small diameter and high aspect ratio.

**Keywords:** Computational fluid dynamics; Micro blowing technique; Skin friction drag; Whole parameters; Active flow control

## INTRODUCTION

Drag reduction has been a classical engineering problem in the field of applied aerodynamics for many years. The modern aircraft engine nacelle is identified as a noteworthy contributor to the total aircraft drag [1], and it is desired to obtain significant engine nacelle drag reduction, while maintaining its overall performance quality and quantity. The major proportion of the total drag is originated from the surface shear stress, which is proportional to the surface area of the aircraft and since the engine nacelle has a large surface area, so the engine drag reduction would bring tremendous benefits to the aircraft. The reduction in aircraft drag has several advantages, such as improved cruise range, lower engine fuel consumption; increased passenger capacity and reduced aircraft direct operating cost [2].

Although new ideas are often being brought up, but in order to be implemented in a transport aircraft, the drag reduction methods are not allowed to add to much weight to the aircraft, otherwise its consequences would overweight the impact of drag reduction. The flow control methods used for drag reduction are the fast-progressing multi-disciplinary technology and can be identified as the future of the aircraft industry [3].

The micro blowing technique termed as MBT, is an active flow control method which reduces wall shear stress by decreasing the velocity profile gradient at the surface wall [4]. The term "micro" implies that the size of the channel hole is much smaller compared to the boundary layer thickness and the micro blowing flow rate needs to be of quite smaller fraction compared to the main stream flow at the boundary layer [5]. The skin friction drags of an ideal micro-porous channel, simulated under

**Correspondence to**: Mushfiq Al Arafa, Department of Science, Computational Engineering, University of Dhaka, Dhaka, Bangladesh, Tel: 8801754958975; E-mail: mushfiq.arafa@ruhr-uni-bochum.de

**Received:** 05-Jan-2022, Manuscript No. JAAE-22-15402; **Editor assigned:** 07-Jan-2022, PreQC No. JAAE-22-15402 (PQ); **Reviewed:** 21-Jan-2022, QC No. JAAE-22-15402; **Revised:** 09-Mar-2022, Manuscript No. JAAE-22-15402 (R); **Published:** 16-Mar-2022, DOI: 10.35248/2168-9792.21.11.285

**Citation:** Arafa MA, Mutekwa M, Chen Z (2022) Influence of Micro-Blowing Technique Hole Parameters on Drag Reduction of Civil Aircraft Engine Nacelle: A Computational Study. J Aeronaut Aerospace Eng. 11:285.

zero blowing velocity should be similar to or less than that of a non-porous surface.

Therefore, the micro blowing concept also provides solution to the large effective surface roughness that arises in normal mass injection method. The large effective surface roughness can be eliminated due to the innovative concept of using very small holes and the turbulent skin friction drag reduction can be obtained by passing an extremely small amount of blowing air at the surface wall of the engine nacelle. The micro blowing technique concept was successful to achieve approximately 50-70% skin friction drag reduction over the engine nacelle, while experiments carried out on operating cruise conditions [6].

The drag reduction is associated and directly proportional on the surface porosity of the surface, e.g., the number of micro- channels, usually low porosity surface is able to reduce the drag by less than 5% [7]. Although few numerical and experimental studies were carried on this unique technique [8] and substantial drag reduction was achieved, but the researchers agreed that the entire aerodynamic characteristic of the highly complex cross flows were not fully understood.

## MATERIALS AND METHODS

### Problem description and design

The engine nacelle boundary layer flow over the entire micro-porous channel will be simulated at operating cruise conditions, using commercial CFD packages to investigate the effect of micro blowing technique on skin friction drag reduction.

The two important parameters of the cruise conditions in this simulation are: flight Mach number and flight crew's altitude [9]. Although different aircraft have their own optimum altitude depending on their individual criteria, but the cruise altitude below 33000 feet has many advantages, as well as the aircrafts fly more economical at Mach numbers below 0.8.

The numerical parametric study will be conducted to analyze the contribution of different MBT configurations on the near wall boundary layer manipulation, hence leading to significant reduction of engine nacelle turbulent skin friction drag. The velocity profile at the downstream of the micro-porous whole region will be extracted, and then compared to investigate the impact of different MBT configurations on the near wall normal velocity gradient.

### Engine nacelle design

The main design requirement of the engine nacelle is to have a suitable aerodynamics shape to avoid excessive drag.

The engine nacelle design used in this paper is inspired from the DLF-F6 engine nacelle configuration, a wind-tunnel model with long duct nacelle feature.

This approximately axisymmetric nacelle geometry is kept accessible for the researchers and has been used during the "AIAA Drag Prediction Workshops" [10]. The nacelle is designed using commercial CAD software (Figure 1A).

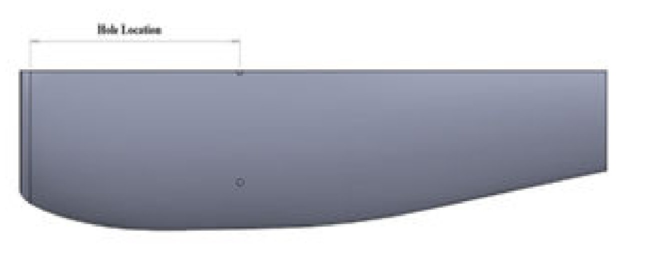


**Figure 1A:** Engine nacelle micro porous whole-location.

The single round micro-porous channels are adapted on the engine nacelle design, as depicted in (Figure 1B) to investigate the flow behavior of the micro-channel jet flow and the macro-cross flow. The single round configuration was adapted instead of the multiple round micro-porous channels. The multiple round channels would require a greater number of iterations to obtain a fully developed flow, hence taking more time to investigate one particular case.

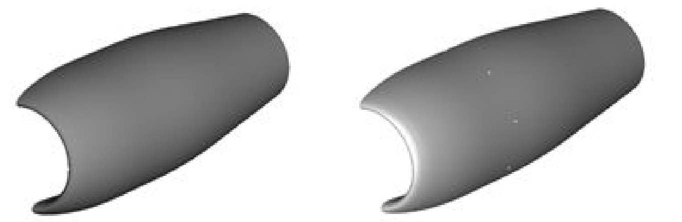

**Figure 1B:** Symmetrical 3D design of engine nacelle solid surface without micro-porous channels (left) and translucent view of micro porous-wholes (right).

### Selection of reference MBT skin

The most important task of the micro blowing technique is to select the proper reference MBT skin which would have an unblown friction drag similar to or less than that of its solid wall [11]. The reference MBT skin would be selected from a pool of different skins, NASA PN2, NASA PN3, GAC2004, GAC2003, GAC2005, GAC2002 and GAC1897 that were analyzed by Hwang at the NASA Lewis Research Center [12]. The configurations with high unblown skin friction coefficient would be eliminated from being an MBT candidate, as they require large amount of blowing air, which is impractical for aircraft application, as aforementioned. The unblown skin-friction of the MBT configurations is shown in (Figure 1C).

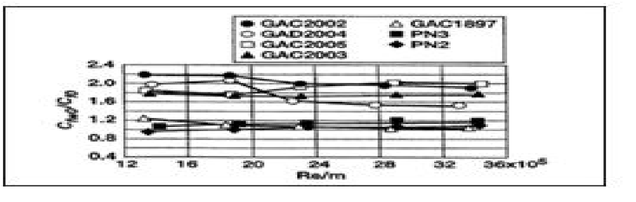


**Figure 1C:** Unblown skin friction ratio.

The first stage of elimination is performed to rule out GAC2002, GAC 2005 and GAC 2003 configurations due to their high unblown high skin friction coefficient. The GAD2004 micro-porous configuration has a high unblown skin friction coefficient at low Reynolds numbers, but it can be expected that it would show better performance at high Reynolds number. But, unfortunately due to lack of adequate experimental data at high Reynolds number, the GAD2004 configuration cannot be chosen. The next configuration to be eliminated is the GAC1897 configuration, and it is due to its hole cross section shape, e.g., hourglass, which is not compatible with our design model.

Therefore, the second stage of elimination rules out the GAD2004 and GAC1897 micro-porous configuration. The NASA PN3 and PN2 configurations are the best two candidates from the list, as they have the unblown skin friction coefficient close of that its solid surface. These two configurations would be able to decrease the skin friction below that of the solid surface even with a very tiny amount of blowing air, which is a necessary requirement to be selected as an MBT skin. The NASA PN2 has to be eliminated at the final stage due to its high whole aspect ratio which cannot be incorporated into the design model.

Therefore, the NASA PN3 is finally chosen as our MBT skin due to its overall compatibility with the design model 9(Table 1A–1D).

**Different MBT configurations**

The MBT configurations are designed by changing one of the hole-parameters at a time from the reference PN3 MBT skin.

The whole aspect ratio and the hole-diameter are the two most important hole-parameters for this research purpose, and since a single row micro channel configuration has been adapted, so the surface porosity was far lower than the reference PN3 configuration.

**Table 1A:** Specification of test cases with variable blowing velocity.

| Name of test configuration | Blowing velocity m/s | Name of test configuration | Blowing velocity m/s | Hole aspect ratio | Hole-diameter mm |
|---|---|---|---|---|---|
| REF00 | Solid wall | BV03 | 2.5 | 4 | 2.5 |
| BV01 | 0 | BV04 | 3.75 | | |
| BV02 | 1.25 | BV05 | 5 | | |

**Table 1B:** Specification of test cases with variable whole-diameter.

| Number of test configuration | Hole-diameter mm | Hole-length mm | Number of test configuration | Hole-diameter mm | Hole-length mm | Hole aspect ratio |
|---|---|---|---|---|---|---|
| HD01 | 1.5 | 6.0 | | | | 4 |
| HD02 | 2.0 | 8.0 | HD04 | 3.0 | 1.2 | |
| HD04 | 3.0 | 1.2 | HD05 | 2.5 | 1.0 | |

**Table 1C:** Specification of test cases with variable hole-diameter.

| Number of test configuration | Hole aspect ratio | Hole-length mm | Number of test configuration | Hole aspect ratio | Hole-length mm | Hole-diameter mm |
|---|---|---|---|---|---|---|
| AR01 | 2 | 5.0 | | | | 2.5 |
| AR02 | 3 | 7.5 | AR04 | 5 | 12.5 | |
| AR03 | 4 | 10.0 | AR05 | 5.5 | 13.75 | |

**Table 1D:** Specification of test cases with variable whole aspect ratio.

| Number of test configuration | Hole location mm | Number of test configuration | Hole location mm | Hole aspect ratio | Hole-diameter mm |
|---|---|---|---|---|---|
| HL01 | 60 | | | 4 | 2.5 |
| HL02 | 70 | HL04 | 90 | | |
| HL03 | 80 | HL05 | 100 | | |

## Computational method

RANS modelling is employed in the present study because of computational resource considerations. The compressible Reynolds-averaged Navier–Stokes equations governing the conservation of mass, momentum and energy are used to describe the turbulent boundary cross flows and it can be written as:

Continuity Equation:

$$\frac{\partial \bar{\rho}}{\partial t} + \frac{\partial}{\partial x_j}(\bar{\rho}\tilde{u}_j) = 0 \quad (3.1)$$

Momentum Equation:

$$\frac{\partial}{\partial t}(\bar{\rho}\tilde{u}_i) + \frac{\partial}{\partial x_j}(\bar{\rho}\tilde{u}_i\tilde{u}_j + \delta_{ij}\bar{p}) = \frac{\partial}{\partial x_j}(\bar{\sigma}_{ij} + \tau_{ij}) \quad (3.2)$$

Energy Equation:

$$\frac{\partial}{\partial t}(\bar{\rho}\tilde{E}) + \frac{\partial}{\partial x_j}[(\bar{\rho}\tilde{E} + \bar{p})\tilde{u}_j] = \frac{\partial}{\partial x_j}[\tilde{u}_i(\bar{\sigma}_{ij} + \tau_{ij}) - (\bar{q}_j + Q_j)] \quad (3.3)$$

The superscript "" denotes the Favre average, and the "–" denotes the Reynolds average. The viscous stress tensor and Reynolds stress tensor seen in the above equations can be elaborated as

$$\bar{\sigma}_{ij} = \tilde{\mu}\left(\frac{\partial \tilde{u}_i}{\partial x_j} + \frac{\partial \tilde{u}_j}{\partial x_i} - \frac{2}{3}\frac{\partial \tilde{u}_k}{\partial x_k}\delta_{ij}\right), \tau_{ij} = \mu_t\left(\frac{\partial \tilde{u}_i}{\partial x_j} + \frac{\partial \tilde{u}_j}{\partial x_i} - \frac{2}{3}\frac{\partial \tilde{u}_k}{\partial x_k}\delta_{ij}\right) - \frac{2}{3}\delta_{ij}\bar{\rho}k \quad (3.4)$$

The heat flux vector and the turbulent heat flux vector are respectively given below:

$$P_k = min\left(\tau_{ij}\frac{\partial U_i}{\partial x_j}, 10\beta^* k\omega\right) \quad (3.9)$$

The kinetic turbulent eddy viscosity is defined by:

$$v_T = \frac{a_1 k}{max(a_1\omega, SF_2)} \quad (3.10)$$

is the second blending function and it is defined by:

$$F_2 = \tanh\left[\left[max\left(\frac{2\sqrt{k}}{\beta^*\omega y}, \frac{500v}{y^2\omega}\right)\right]^2\right] \quad (3.11)$$

$$\bar{q}_j = -\tilde{\kappa}\frac{\partial \tilde{T}}{\partial x_j}, Q_j = -\kappa_t\frac{\partial \tilde{T}}{\partial x_j} \quad (3.5)$$

The -ω shear stress transport (SST) model is the most suitable RANS turbulence model for this research approach [13,14]. This model has the ability to switch between -omega and -epsilon turbulence model, such that k-omega can implemented to capture the flow structure in inner region of the boundary layer and k-epsilon in the free stream region [15]. The governing equations of –ω SST model was first proposed by Menter and it is given as follow [16].

Turbulent Kinetic Energy:

$$\frac{\partial k}{\partial t} + U_j\frac{\partial k}{\partial x_j} = P_k - \beta^* k\omega + \frac{\partial}{\partial x_j}\left[(v + \sigma_k v_T)\frac{\partial k}{\partial x_j}\right] \quad (3.6)$$

Specific Dissipation Rate:

$$\frac{\partial \omega}{\partial t} + U_j\frac{\partial \omega}{\partial x_j} = \alpha S^2 - \beta\omega^2 + \frac{\partial}{\partial x_j}\left[(v + \sigma_\omega v_T)\frac{\partial \omega}{\partial x_j}\right] + 2(1 - F_1)\sigma_{\omega 2}\frac{1}{\omega}\frac{\partial k}{\partial x_i}\frac{\partial \omega}{\partial x_i} \quad (3.7)$$

Where the blending function is defined by:

$$F_1 = \tanh\left\{\left\{min\left[max\left(\frac{\sqrt{k}}{\beta^*\omega y}, \frac{500v}{y^2\omega}\right), \frac{4\sigma_{\omega 2}k}{CD_{k\omega}y^2}\right]\right\}^4\right\} \quad (3.8)$$

With $CD_{kw} = max\left(2\rho\sigma_{\omega 2}\frac{1}{\omega}\frac{\partial k}{\partial x_i}\frac{\partial \omega}{\partial x_i}, 10^{-10}\right)$, and y is the nearest wall distance.

## Model pre-processing–mesh

The mesh quality is an important factor to be maintained in order to obtain adequate simulation accuracy in computational fluid dynamics [13]. Although there is no specific rule of thumb to construct a fine mesh, but there are some important mesh parameters, e.g., skewness, orthogonality, aspect ratio, etc. which can imply that the mesh resolution is sufficiently fine to provide a precise solution (Figure 2A).

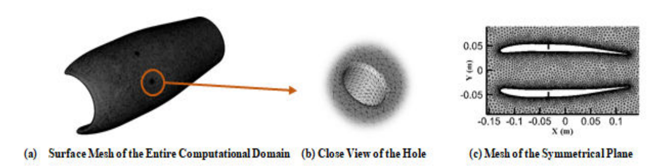


**Figure 2A:** Mesh details of the computational domain.

The mesh details of the computational domain of the engine nacelle and at the vicinity of the micro porous hole are shown in (Figure 2B). The near wall region of the channels is modeled with high number of mesh elements, so that the boundary layer can be solved efficiently. The volume mesh on the symmetrical plane shows the growth of the mesh around the engine surface, and there is no sign of abrupt change in the mesh density. The maximum skewness value is far below the margin of 0.95 and the minimum orthogonality quality is above 0.1, which are the minimum requirement for a good mesh.

**Grid independence study:** The convergence of the numerical solution is not sufficient enough to ensure that the solution results are acceptable, it is also required to investigate that the solution is independent of the mesh resolution [14]. In general, the accuracy of the results depend on how accurately the contour of the geometry can be captured, but on the other hand, due to limited computational resources, there is a limitation of the mesh elements that can be used to define the geometry (Figure 2B).

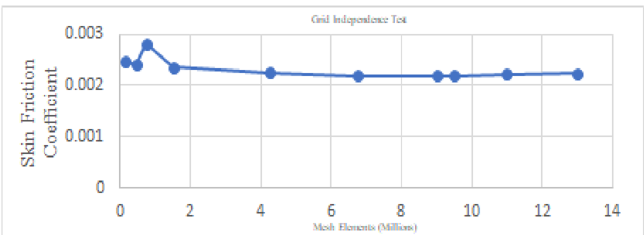


**Figure 2B:** Skin friction coefficient varition with increasing mesh resolution.

The results in (Figure 2B) show that at the initial stage, by increasing the mesh elements, there is a significant change in the skin friction coefficient. The results varied widely below 2 million cells, implying that the simulation results are dependent on the mesh elements. Further increment of the mesh elements did not show any sign of abrupt change in the skin friction coefficient value, indicating that the solution value is independent of the mesh elements. Therefore, according to the graph, the mesh elements of approximately 8-10 million cells are adequate enough for our simulation.

# RESULTS

## Numerical simulation and result analysis

The main objective of this computational analysis is to investigate the effect of the three major whole parameters, hole-aspect ratio, hole-diameter and blowing velocity on the skin friction drag reduction.

Another whole parameter, whole-location is believed to have minimal impact on the skin friction drag, therefore, in order to ensure this hypothesis, a sensitivity study will be carried out at the beginning to eliminate it out of the whole parameters.

The solid engine nacelle surface is chosen as the baseline model to compare the effects of the whole parameters, blowing velocity, whole aspect ratio, and whole diameter in skin friction drag reduction.

The porosity of the engine nacelle is much less than the reference MBT skin NASA PN3 (porosity 23 %) so it is quite obvious that our designed model would not be able to achieve less drag reduction compared to its pioneers. Therefore, it is not logical to make direct comparison in drag reduction capabilities between them.

The trend of the drag reduction would be compared between these cases, as the characteristics of the flow field would be similar.

**Sensitivity study of whole location:** The sensitivity study is carried out to observe the effect of the micro-porous whole location on skin friction drag reduction, as presented in the whole location is measured from a specific point of the leading edge of the engine nacelle as shown in (Figure 2A).

It can be observed from the graph, as postulated before that the whole location does not have a great impact on the skin friction reduction, therefore, it can be excluded from being an important whole parameter.

The velocity streamline of the channel flows with variable whole location configuration, presented in (Figure 3A) shows that all the configurations have similar type of vortical structures formed inside the hole.

The skin friction coefficients of all the test configurations are listed in (Table 2A), and it can be observed that almost all the test configurations were able to achieve the same amount of drag reduction.

The HL04 configuration unexpectedly showed a small deflection of 0.05% from the average drag reduction value, although it is small enough to be considered as negligible.

The velocity profile of the test configurations in (Figure 3B) exhibits a similar velocity gradient within the boundary layer.

Therefore, from the above discussion it can be stated that the particular whole location should be finalized by considering the other factors related to the engine nacelle.

The position of the pylon, shown in (Figure 2A), covers approximately one-third of the upper surface of the engine nacelle, therefore, is one of the most important factors to be considered to determine the particular position of the wholes.

**Table 2A:** Skin friction drag reduction with variable whole location.

| Name of test configuration | Hole location mm | Skin friction coefficient | Drag reduction (percentage | Name of test configuration | Hole location mm | Skin friction coefficient | Drag reduction (percentage |
|---|---|---|---|---|---|---|---|
| HL01 | 60 | 0.0022217 | 7.329 | | | | |
| HL02 | 70 | 0.0022218 | 7.325 | HL04 | 90 | 0.0022285 | 7.045 |
| HL03 | 80 | 0.0022166 | 7.542 | HL05 | 100 | 0.0022156 | 7.583 |

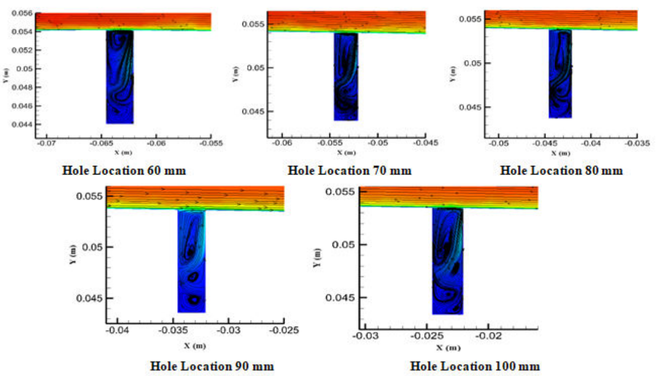


**Figure 3A:** Streamlines of the flow with variable whole location and constant whole diameter and aspect ratio with blowing velocity of 0 m/s around the micro-porous channel.

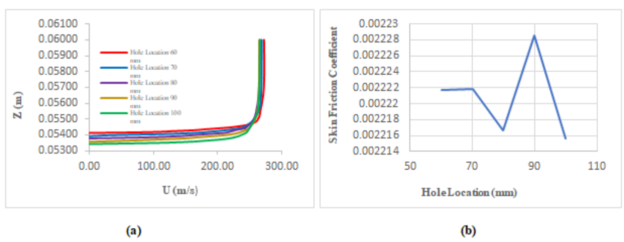


**Figure 3B:** Effect of whole location on (a) velocity profile and (b) skin friction coefficient.

**Impact of blowing velocity:** The blowing velocity, manipulates the velocity slope of the cross flow and reduces the surface roughness, eventually making a magnificent impact on the skin friction drag reduction. Although, the mixing zone created due to the main stream flow and micro-porous flow is quite small compared to the boundary layer thickness, but it is adequate enough to manipulate the boundary layer at the vicinity of the engine nacelle surface. The variation of the skin friction drag against the blowing velocity is presented in (Figure 3C), despite of having a single-row micro porous configuration; the drag is reduced around 8%, which is quite significant. The micro blowing technique is able to achieve drag reduction as the blowing velocity is increased up to a certain value; in this case it is observed from (Table 2B), that the optimum drag reduction velocity configuration is BV03, at 2.5 m/s.

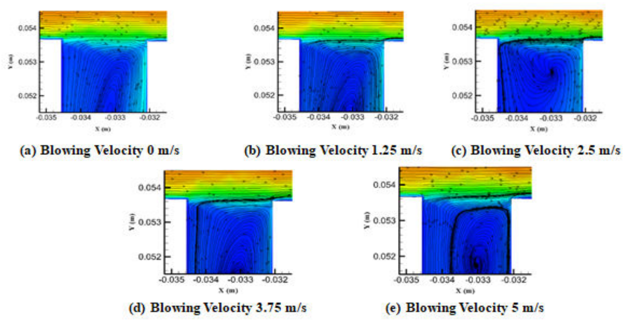


**Figure 3C:** Streamline of the cross flow around the micro-porous whole.

The BV01 configurations with blowing velocity of 0 m/s as presented in (Figure 3D), shows that the main stream flow is undisturbed as there is no injection of air from the micro-porous channel. The velocity streamlines of BV02 configuration shows that, this test case has a smaller amount of air injected into the main stream flow, thus the disturbance induced in the cross-flow is negligible. The test configuration BV03, and its boundary layer flow shown in (Figure 3E) a-f, implies that the boundary layer thickness is increased as the blowing air is injected and an intermediate layer is created between the engine nacelle surface and the boundary layer. This phenomenon of separating the boundary layer is the most unique feature of micro blowing technique, and eventually it reduces the velocity gradient resulting in skin friction drag reduction, as presented in (Figure 3F). The blowing velocity above 2.5 m/s shows complex axisymmetric vortex at the downstream edge of the hole, as the vortex structures are unsteady, so it cannot be analyzed with this steady state simulation study. The path line of the micro-jet flow from the whole channel at different blowing velocity is represented in (Figure 3G), (Table 2B).

**Table 2B:** Skin friction drag reduction with variable blowing velocity.

| Name of test configuration | Blowing velocity m/s | Skin friction coefficient | Drag reduction (percentage) | Name of test configuration | Blowing velocity m/s | Skin friction coefficient | Drag reduction (percentage) |
|---|---|---|---|---|---|---|---|
| REF00 | Solid wall | 0.0023974 | Baseline | BV03 | 2.5 | 0.0021996 | 8.251 |
| BV01 | 0 | 0.0022285 | 7.045 | BV04 | 3.75 | 0.0022218 | 7.483 |
| BV02 | 1.25 | 0.0022276 | 7.083 | BV05 | 5 | 0.0022241 | 7.229 |

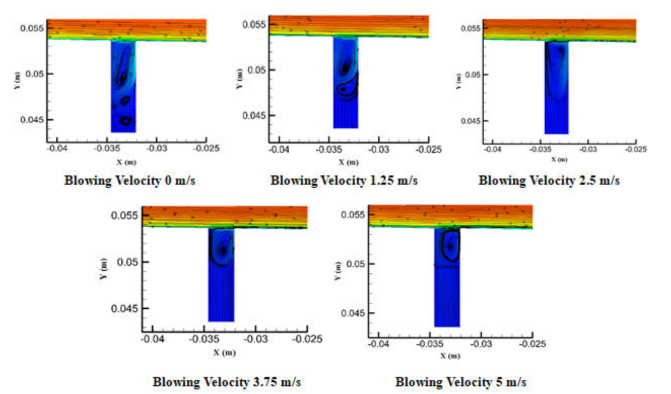


**Figure 3D:** Streamlines of the flow with variable blowing velocity around the micro-porous channel.

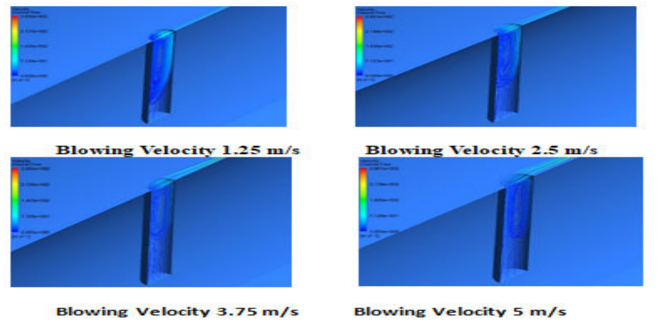


**Figure 3G:** The path line of the flow characteristics from the symmetrical plane micro-porous holes at variable blowing velocity.

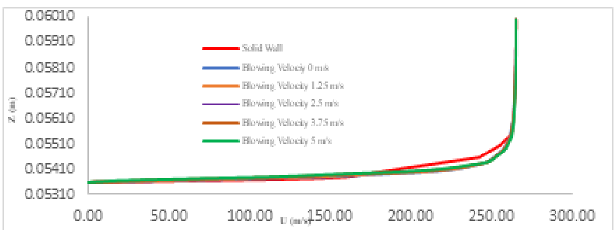


**Figure 3E:** Effect of blowing velocity on velocity profile.

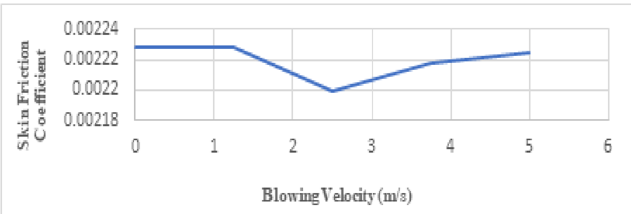


**Figure 3F:** Effect of blowing velocity on skin friction coefficient.

**Impact of whole aspect ratio:** The variation of the skin friction coefficient against the variable whole aspect ratio is presented in (Figure 3H, 3I), it shows impact of the whole aspect ratio on the skin friction coefficient.

The velocity profiles of all the test configurations at the downstream section of the micro-porous zone are presented in (Figure 3J) to investigate the effect of whole aspect ratio.

The test configurations shown in (Table 2C) are simulated with a constant whole diameter, 2.5 mm (reference MBT skin -NASA PN3) and zero blowing velocity.

The results follow the same trend as shown in Fig 2.4, the drag reduction is less at low aspect ratio and the drag reduction increases as the aspect ratio is increased.

The drag reduction is approximately similar for the configurations with aspect ratio above 2, and the highest drag reduction of approximately 7 % is achieved with the aspect ratio of 5.5. For high aspect ratio configurations above 2, there are several vortices formed inside the hole and it implies that the boundary layer flow is prevented from entering the hole.

The vortices form a smooth layer which relatively low effective surface roughness compared to the solid engine nacelle surface over which the boundary layer flows and thus resulting in reduction of skin friction drag. Therefore, from this computational analysis, it can be stated that a high aspect ratio is preferable for our MBT configuration.

But in terms of practical usage in aircraft applications, aspect ratio above 4 would not be compatible to be incorporated inside the engine nacelle, because a small margin of space is left for the mechanical devices to be installed to drive the blowing air (Table 2C).

Table 2C: Skin friction drag reduction with different aspect ratio.

| Name of test configuration | Aspect ratio | Skin friction coefficient | Drag reduction (percentage) | Name of test configuration | Aspect ratio | Skin friction coefficient | Drag reduction (percentage) |
|---|---|---|---|---|---|---|---|
| AR01 | 2 | 0.0022671 | 5.435 | | | | |
| AR02 | 3 | 0.0022241 | 7.229 | AR04 | 5 | 0.0022257 | 7.162 |
| AR03 | 4 | 0.0022285 | 7.045 | AR05 | 5.5 | 0.0022217 | 7.329 |

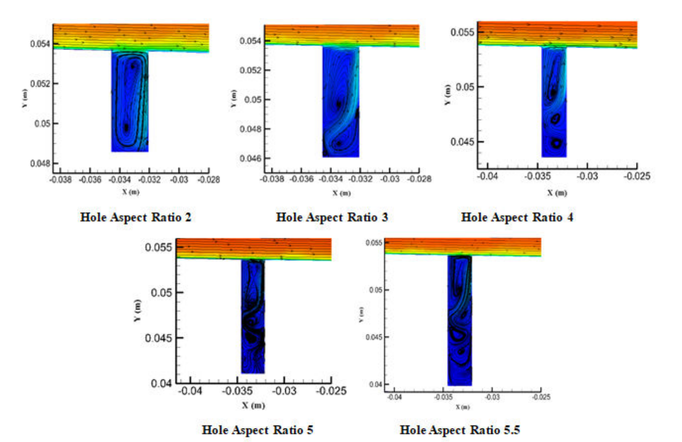


**Figure 3H:** Streamlines of the flow with variable whole aspect ratio and constant hole diameter with blowing velocity of 0 m/s around the micro-porous channel.

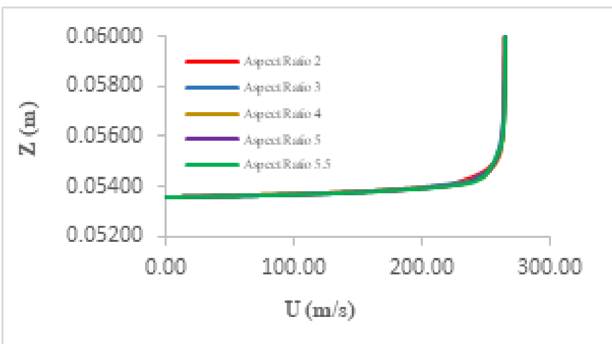


**Figure 3I:** Effect of aspect ratio on velocity profile.

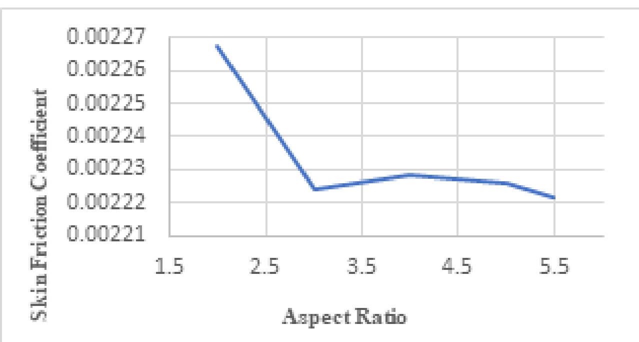


**Figure 3J:** Effect of aspect ratio on skin friction coefficient.

**Impact of whole Diameter:** The skin friction coefficient is plotted against variable whole diameter, as presented in (Figure 3K) to investigate the effect of the whole diameter. The velocity profile for the test configurations is depicted in (Figure 3L), and it clearly shows the difference between the velocity profile of the small and large whole diameter configurations at the downstream section of the micro-porous hole. The velocity streamlines of the channel flow, as shown in (Figure 3M), clearly shows the complex vortical structures formed inside the flow. The main stream flow over the effective surface formed by these vortices is practically undistorted for the small whole diameter configurations.

As the whole diameters are gradually increased, the boundary layer has a greater possibility to enter and accumulate at the downstream edge of the micro-porous hole. This stagnation would eventually increase the overall effective surface roughness and establish greater shear stress between the vortical structures and the main stream flow, resulting in increment of the skin friction drag. Therefore, the configurations with smaller whole diameter were able to achieve substantial skin friction drag reduction, and as the whole diameter is gradually increased, the drag reduction becomes lesser. But on the other hand, if we consider the case, where the engine nacelle surface has a high porosity of approximately 23% as seen for the NASA PN3 configuration, then a large number of micro porous holes would be required. Therefore, a trade-off needs to be made between the number of holes and the optimum whole diameter to maintain a high surface porosity.

The HD01 configuration, which has the whole diameter of 1.5 mm, has made the highest drag reduction of approximately 7.5 % than its solid surface. The following HD02 configuration also shows similar percentage of drag reduction and it is most likely to be chosen in practical applications. At the same time, a good amount of drag reduction can also be achieved with higher whole diameter, but as aforementioned before, these large whole configurations are quite impractical for aircraft applications and it would be almost impossible to be incorporated into the engine nacelle surface. Therefore, from this numerical investigation, it can be concluded that smaller holes are preferred for the MBT skins and the exact size can be determined considering the surface porosity and the number of micro-holes (Table 2D).

**Table 2D:** Skin friction drag reduction with variable hole-diameter.

| Name of test configuration | Hole-diameter mm | Skin friction coefficient | Drag reduction (percentage) |
|---|---|---|---|
| HD01 | 1.5 | 0.0022178 | 7.491 |
| HD02 | 2.0 | 0.0022187 | 7.454 |
| HD03 | 2.5 | 0.0022285 | 7.045 |
| HD04 | 3.0 | 0.0022265 | 7.129 |
| HD05 | 3.5 | 0.0022496 | 6.165 |

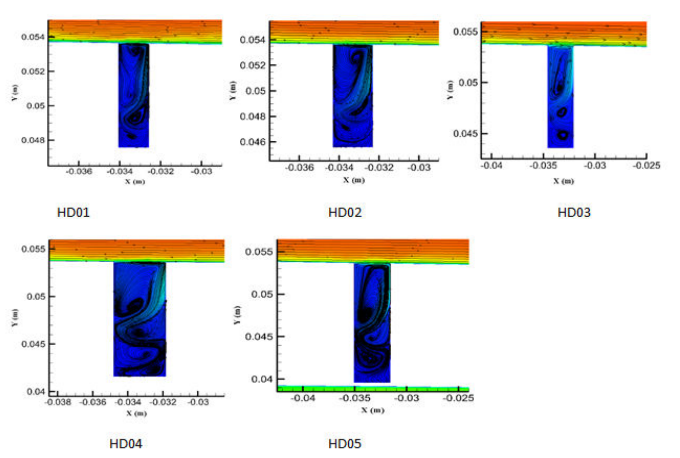


**Figure 3K:** Streamlines of the flow with variable whole diameter and constant whole aspect ratio with blowing velocity of 0 m/s around the micro-porous channel.

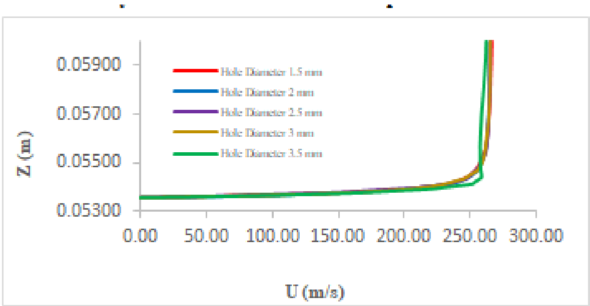


**Figure 3L:** Effect of whole diameter on velocity profile.

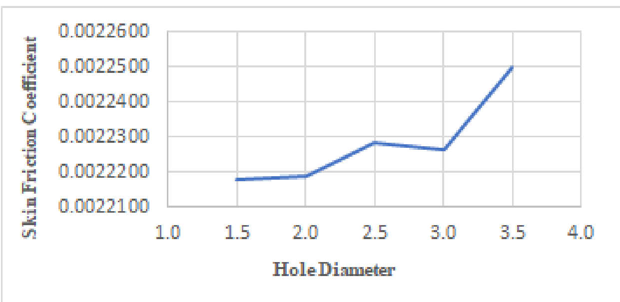


**Figure 3M:** Effect of whole diameter on skin friction coefficient.

## DISCUSSION

The micro blowing technique is capable to reduce the skin friction drag over the engine nacelle surface by decreasing the velocity gradient, e.g., lessening the near wall normal velocity gradient inside the boundary layer and providing low effective surface roughness over the micro-porous holes. The computational parametrical investigation was carried out at cruise conditions to analyze the effect of the micro blowing velocity and its major whole parameters, e.g. aspect ratio and diameter on the skin friction drag reduction. The hole location is another hole-parameter, which does not have a great impact on skin friction drag reduction, therefore, the particular position of the micro-porous holes are selected based on the position of the pylon over the engine nacelle.

The simulation results obtained by solving the Reynolds average Navier-Stokes equation has shown similar trend of the results with the previous works on micro blowing technique. The results establish that drag reduction can be achieved by blowing a small amount of air into the boundary layer, the drag reduction increases as the blowing velocity is increased up to a certain point, after which the increment of the velocity results in increased drag.

## CONCLUSION

The parametric study also revealed that the skin friction drag reduction is heavily linked with the whole parameters. The impact of the whole diameter and whole aspect ratio are maximum when smaller hole diameter and higher hole aspect ratio are used respectively. The micro blowing technique was able to substantially reduce the skin friction drag by 7-8%, keeping in mind that a small surface porosity was used. The drag reduction results are believed to be improved by adding more channels, e.g., implementing the multi-channel configuration, thus increasing the overall surface porosity.

Further analysis can be carried out to investigate the vortical structures formed at the vicinity of the downstream of the micro-porous holes and to fully validate the numerical results with experimental analysis on a physical model.

## DECLARATION

The authors declare no conflict of interest.

# REFERENCES


1. Robinson M, MacManus D, Sheaf C. Aspects of aero-engine nacelle drag proceedings of the Institution of Mechanical Engineers. Part G. J Aero Eng. 2018.
2. Tillman TG, Hwang DP. Drag reduction on a large-scale nacelle using a micro-blowing technique. AIAA Paper AIAA–99–0130. 1999.
3. Malik MR, Crouch JD, Saric WS, Lin JC, Whalen EA. Application of drag reduction techniques to transport aircraft. New Jersey, John Wiley & Sons, Ltd. 2015.
4. Atzori M, Vinuesa R, Fahland G, Stroh A, Gatti D, Frohnapfel B, et al. Aerodynamic Effects of Uniform Blowing and Suction on a NACA4412 Airfoil. Flow, Turbulence and Combustion. 2020;1-25.
5. Hwang D. Experimental Study of Characteristics of Micro-Hole Porous Skins for Turbulent Skin Friction Reduction. 2002.
6. Kornilov VI, Boiko A. Flat-plate drag reduction with streamwise noncontinuous microblowing. AIAA. 2014;52(1):93-103.
7. Li J, Lee CH, Jia L, Li X. Numerical study on flow control by micro-blowing. In 47th AIAA Aerospace Sciences Meeting including The New Horizons Forum and Aerospace Exposition. 2009;779.
8. Kudriavtsev V, Braun M. Computational Study of Micro-Blowing for Shear Force Reduction. Computational Technologies for Fluid/Thermal/Structural/Chemical Systems with Industrial Applications. 2001;2.
9. Jiang S, Luo X, He . Research on Method of Trajectory Prediction in Aircraft Flight Based on Aircraft Performance and Historical Track Data. Math Probl Eng. 2021.
10. Applied Aerodynamics T. 2nd AIAA CFD Drag Prediction Workshop. 2003.
11. Hwang DP. Skin-friction reduction by a micro-blowing technique. AIAA. 1998;36(3):480-481.
12. Hwang D, Hwang D. A proof-of-concept experiment for reducing skin friction by using a micro-blowing technique. 35th Aerospace Sciences Meeting and Exhibit. 1997;546.
13. Adumiotroaie V, Ristorcelli JR, Taulbee DB. Progress in Fabré-Reynolds Stress Closures for Compressible Flows. ICASE Rpt. 1998;98-121.
14. ANSYS FLUENT. Theory Guide - 4.12.1 Overview. 2021.
15. Menter FR, Kuntz M, Langtry R. Ten Years of Industrial Experience with the SST Turbulence Model. Turbulence, Heat and Mass Transfer 4, K. Hanjalic, Y. Nagano, and M. Tummers (eds.), Begell House Inc. 2003.
16. Lee M, Park G, Park C, Kim C. Improvement of Grid Independence Test for Computational Fluid Dynamics Model of Building Based on Grid Resolution. Adv Civ Eng. 2020.